Decoherence of a two-qubit system away from perfect symmetry

M. J. Storcz,* F. Hellmann, C. Hrelescu, and F. K. Wilhelm
Physics Department, Arnold Sommerfeld Center for Theoretical Physics, and Center for NanoScience, Ludwig-Maximilians-Universität München, Theresienstrasse 37, 80333 München, Germany
(Received 13 June 2005; published 14 November 2005)

The decoherence of an asymmetric two-qubit system that is coupled via a variable interaction term to a common bath or two individual baths of harmonic oscillators is examined. The dissipative dynamics are evaluated using the Bloch-Redfield formalism. It is shown that the behavior of the decoherence effects is affected mostly by the symmetries between the qubit operator that is coupled to the environment and the temperature, whereas the differences between the two bath configurations are very small. Moreover, it is elaborated that small imperfections of the qubit parameters do not necessarily lead to a drastic enhancement of the decoherence rates.

DOI: 10.1103/PhysRevA.72.052314 PACS number(s): 03.67.Lx, 03.65.Yz, 05.40.−a, 85.25.−j

I. INTRODUCTION

Quantum computation provides a substantial speedup for several important computational tasks [1–4]. A general quantum bit (qubit) consists of a two level quantum system with a controllable Hamiltonian of sufficient generality to implement a universal set of quantum logic gates [5]. From such a set, an arbitrary quantum algorithm can be implemented to any desired accuracy limited only by decoherence. A universal two qubit system requires just single-qubit rotations and one additional entangling two qubit gate. One important example for an entangling two qubit gate is the controlled-NOT (CNOT) gate that switches the state of the second qubit depending on the state of the first qubit.

Superconducting Josephson charge and persistent current (flux) qubits have been shown to possess the necessary properties [4] to act as quantum bits. They have been manipulated coherently and coherence times in the μs range have been demonstrated experimentally [6–12] with a corresponding quality factor of quantum coherence of up to $Q_\varphi \approx 10^4$ [10]. In a two qubit system, where the coupling was achieved using a shared Josephson junction, coherent Rabi oscillations between states of a coupled qubit system were observed [13,14] and in a two charge qubit system a conditional gate operation was performed [12]. All of these experiments suffer from material imperfections which lead to nonideal time evolutions of the quantum states due to a parameter spread in the characteristic energies of the system Hamiltonian. Thus, it is of general importance to theoretically model these asymmetric qubit systems and their decoherence properties to optimize the decoherence in experimental setups. In this paper, the dependence of the decoherence rates and gate quality factors on the parameter spread of the qubits will be elaborated theoretically. In perspective, this is of crucial importance for connecting the experimental status and prospects to these central concepts in quantum information science: which degree of parameter uniformity do experiments have to achieve for symmetry-based protection schemes to work—do these schemes have to be extended in order to accomodate experimental restrictions?

On the other hand, for high symmetry of the qubit parameters, the qubit coherence can be intrinsically strongly protected. This extends from the protection of the singlet in a symmetric qubit setup [15] to the general concept of decoherence-free subspaces (DFS's) [16,17]. General considerations on the stability of such DFS's can be found in Ref. [18]. In this paper the experimental conditions for these intrinsic protection mechanisms are investigated and direct conclusions for the decoherence of a two qubit system are given.

Also, variable bath couplings to the decohering environment have already been identified as a novel parameter for engineering decoherence, e.g., in Ref. [19]. It is exactly these decoherence properties of a qubit bath interaction operator that lies in the xz plane on the Bloch sphere that will be investigated in this work.

In Sec. II, we will introduce the global model of two qubits with a general bath coupling operator and how coherence can be protected by symmetry. In Sec. III, we specify how decoherence is parameterized and handled using the Bloch-Redfield approach, which helps to compute the gate quality factors introduced in Sec. IV. Results are summarized in the two subsequent sections: Section V shows how decoherence and gate quality depends on the coupling angle whereas Sec. VI discusses the experimentally important case of asymmetrically fabricated qubits.

II. THE MODEL

The Hamiltonian of a typical pseudo-spin system can be expressed in terms of the Pauli matrices as

$$\mathbf{H}_q = -\frac{1}{2}(\epsilon\hat{\sigma}_z + \Delta\hat{\sigma}_x), \tag{1}$$

where ϵ is the energy bias and Δ is the tunneling amplitude. In a two qubit system, an additional interaction term is required to implement the universal two qubit gate. In superconducting implementations [6,8–11,20,21] this coupling

*Email address: storcz@theorie.physik.uni-muenchen.de

term is typically proportional to $\hat{\sigma}_z^{(1)}\hat{\sigma}_z^{(2)}$. Here, the superscripts are the qubit indices. In particular, inductively coupled flux qubits [15,22] and capacitively coupled charge qubits [23] are coupled this way. Thus, the two qubit Hamiltonian is

$$\mathbf{H}_{2q} = -\frac{1}{2}\sum_{i=1}^{2}(\epsilon^{(i)}\hat{\sigma}_z^{(i)} + \Delta^{(i)}\hat{\sigma}_x^{(i)}) - \frac{\gamma}{2}\hat{\sigma}_z^{(1)}\hat{\sigma}_z^{(2)}. \tag{2}$$

In the singlet/triplet basis, $(1,0,0,0)^T = |\uparrow\uparrow\rangle$, $(0,1,0,0)^T = (|\uparrow\downarrow\rangle + |\downarrow\uparrow\rangle)/\sqrt{2}$, $(0,0,1,0)^T = |\downarrow\downarrow\rangle$, $(0,0,0,1)^T = (|\uparrow\downarrow\rangle - |\downarrow\uparrow\rangle)/\sqrt{2}$ that exhibits the symmetry properties of the coupling most clearly, this Hamiltonian takes the following explicit matrix form:

$$\mathbf{H}_{2q} = -\frac{1}{2}\begin{pmatrix} \epsilon & \eta & \gamma & -\Delta\eta \\ \eta & -\gamma & \eta & -\Delta\epsilon \\ \gamma & \eta & -\epsilon & \Delta\eta \\ -\Delta\eta & -\Delta\epsilon & \Delta\eta & \gamma \end{pmatrix}, \tag{3}$$

with $\epsilon = \epsilon^{(1)} + \epsilon^{(2)}$, $\Delta\epsilon = \epsilon^{(1)} - \epsilon^{(2)}$ and $\eta = (\Delta^{(1)} + \Delta^{(2)})/\sqrt{2}$, $\Delta\eta = (\Delta^{(1)} - \Delta^{(2)})/\sqrt{2}$. Using this Hamiltonian the CNOT gate can be implemented through a sequence of elementary quantum gates [15,24]

$$U_{\mathrm{CNOT}} = U_{\mathrm{H}}^{(2)} \exp\left(-i\frac{\pi}{4}\hat{\sigma}_z^{(1)}\right)\exp\left(-i\frac{\pi}{4}\hat{\sigma}_z^{(2)}\right) \times \exp\left(-i\frac{\pi}{4}\hat{\sigma}_z^{(1)}\sigma_z^{(2)}\right)\exp\left(-i\frac{\pi}{2}\hat{\sigma}_z^{(1)}\right)U_{\mathrm{H}}^{(2)}, \tag{4}$$

where $U_{\mathrm{H}}^{(2)}$ denotes the Hadamard gate operation performed on the second qubit. It involves one two-qubit operation at step three only. For our numerical calculations we applied the characteristic energies that were used in Ref. [15] as a viable example for superconducting solid-state flux or charge qubits. Following this approach also gate sequences optimized with respect to decoherence have been studied [25]. Disregarding the Hadamard gates, the gate operation Eq. (4) forms a controlled-phase (CPHASE) gate

$$U_{\mathrm{CPHASE}} = \begin{pmatrix} 1 & 0 & 0 & 0 \\ 0 & 1 & 0 & 0 \\ 0 & 0 & 1 & 0 \\ 0 & 0 & 0 & e^{i\phi} \end{pmatrix}, \tag{5}$$

with $\phi = \pi$.

III. DECOHERENCE

In experimental realizations of this model, additional effects always impair the capability of the system to operate as a qubit. In condensed matter implementations, the most pronounced is the coupling to environmental degrees of freedom. This leads to relaxation, i.e., classical thermalization of the states as well as, on a much shorter time scale, to dephasing. Decoherence causes the system to act similar to a classical ensemble eliminating all potential computational benefits of quantum algorithms. For a wide range (e.g, Refs. [15,23,26]) of solid state implementations the dominant decoherence effects caused by coupling to linear environments such as electric circuits obey Gaussian statistics and can be effectively modeled with a bath of harmonic oscillators. It is assumed here that there is only one decoherence source in the dominating order of magnitude in the coupling parameter and possible weaker noise sources are ignored. To model this source each qubit is either coupled to an individual or to a common bath of harmonic oscillators. The system Hamiltonian then takes the form

$$\mathbf{H}_{2\mathrm{qB}}^{2\mathrm{B}} = \mathbf{H}_{2q} + \frac{1}{2}(\hat{\sigma}_s^{(1)}\hat{X}^{(1)} + \hat{\sigma}_s^{(2)}\hat{X}^{(2)}) + \mathbf{H}_B^{(1)} + \mathbf{H}_B^{(2)} \tag{6}$$

or

$$\mathbf{H}_{2\mathrm{qB}}^{1\mathrm{B}} = \mathbf{H}_{2q} + \frac{1}{2}(\hat{\sigma}_s^{(1)} + \hat{\sigma}_s^{(2)})\hat{X} + \mathbf{H}_B, \tag{7}$$

where $\hat{\sigma}_s$ is the spin representation of the qubit operator talking to the environment that depends on the specific implementation of the qubit. For the special case of superconducting flux qubits, which only experience flux noise, and superconducting charge qubits which are only subject to charge noise, this would correspond to $\hat{\sigma}_s = \hat{\sigma}_z$. Here, $\hat{X}$ is the collective coordinate of the harmonic oscillator bath and the superscript distinguishes between the single bath and the two bath case. The general form is

$$\hat{\sigma}_s = (\vec{c}\cdot\vec{\sigma}) = \sqrt{2}(c_x\hat{\sigma}_x + c_y\hat{\sigma}_y) + c_z\hat{\sigma}_z, \tag{8}$$

where the factor $\sqrt{2}$ in front of c_x and c_y was chosen for convenience in the singlet/triplet basis in which the qubit-bath interaction becomes

$$\mathbf{H}_{\mathrm{int}} = \frac{1}{2}\begin{pmatrix} c_z\hat{X} & c_-\hat{X} & 0 & -c_-\Delta\hat{X} \\ c_+\hat{X} & 0 & c_-\hat{X} & c_z\Delta\hat{X} \\ 0 & c_+\hat{X} & -c_z\hat{X} & c_+\Delta\hat{X} \\ -c_+\Delta\hat{X} & c_z\Delta\hat{X} & c_-\Delta\hat{X} & 0 \end{pmatrix}, \tag{9}$$

with $c_\pm = c_x \pm ic_y$, $\hat{X} = \hat{X}^{(1)} + \hat{X}^{(2)}$. Here, $\Delta\hat{X} = \hat{X}^{(1)} - \hat{X}^{(2)}$ for the case of two baths and $\Delta\hat{X} = 0$ for one common bath.

In the following we will, without loss of generality, characterize the results by the angle θ between the $\hat{\sigma}_x$ and $\hat{\sigma}_z$ component of the coupling

$$\hat{\sigma}_s\hat{X} = (\hat{\sigma}_x \sin\theta + \hat{\sigma}_z\cos\theta)\hat{X}. \tag{10}$$

This is completely analogous to the bath coupling that is encountered in proposed experimental qubit realizations, e.g., for charge qubits [19]. The bath coupling angle θ is defined for $\theta \in [0, \pi/2]$.

Following the lines of Refs. [15,26], the Bloch-Redfield formalism is applied to calculate the effects of decoherence. The Bloch-Redfield equations and decoherence rates are given analytically. However, in comparsion to a fully analytic evaluation of the dynamics of the two-qubit system [27], with this method the time evolution of the reduced density matrix can also be determined numerically for a wide range of system Hamiltonians.

The environment, i.e., the bath of harmonic oscillators, is characterized by its spectral density. The strength of the dissipative effects is given by the dimensionless parameter α. The bath spectral function is assumed to be linear in frequency up to a cutoff frequency ω_c. Thus, $J(\omega)=\alpha\hbar\omega/[1+(\omega/\omega_c)^2]$, i.e., we employ an Ohmic spectrum with a Drude cutoff. The cutoff frequency is chosen two orders of magnitude above the largest frequency which is typical for a flux qubit system, $\omega_c=10^{13}$ Hz [7].

We choose a rather large coupling strength to the environment of $\alpha=10^{-3}$, which is still in the weak coupling regime, to be able to observe pronounced decoherence effects. The Bloch-Redfield equations describe the evolution of the density matrix in the eigenbasis of the unperturbed Hamiltonian [28,29]

$$\dot{\rho}_{nm} = -i\omega_{nm}\rho_{nm} - \sum_{kl} R_{nmkl}\rho_{kl}, \tag{11}$$

where the Redfield tensor R_{nmkl} is given by

$$R_{nmkl} = \delta_{lm}\sum_r \Gamma^{(+)}_{nrrk} + \delta_{nk}\sum_r \Gamma^{(-)}_{lrrm} - \Gamma^{(-)}_{lmnk} - \Gamma^{(+)}_{lmnk}, \tag{12}$$

and the rates Γ are given by the Golden Rule expressions

$$\Gamma^{(+)}_{lmnk} = \hbar^{-2}\int_0^\infty dt e^{-i\omega_{nk}t}\langle \tilde{H}_{I,lm}(t)\tilde{H}_{I,nk}(0)\rangle_\beta, \tag{13}$$

$$\Gamma^{(-)}_{lmnk} = \hbar^{-2}\int_0^\infty dt e^{-i\omega_{lm}t}\langle \tilde{H}_{I,lm}(0)\tilde{H}_{I,nk}(t)\rangle_\beta, \tag{14}$$

where $\tilde{H}_{I,ij}(t)$ is the matrix element of the bath/system coupling part of the Hamiltonian in the interaction picture. Here, β indicates averaging over the degrees of freedom of the thermal bath. In the following $\beta=1/k_BT$, where T is the temperature of the bath. Evaluating this, we find according to Ref. [15] for one common bath the rates

$$\Gamma^{(\pm)}_{lmnk} = \frac{1}{8\hbar}\Lambda J(\omega_{ab})[\coth(\beta\hbar\omega_{ab}/2)\mp 1] + \frac{i\Lambda}{4\pi\hbar} \times \mathcal{P}\int_0^\infty d\omega \frac{J(\omega)}{\omega^2-\omega_{ab}^2}[\coth(\beta\hbar\omega/2)\omega_{ab}\mp\omega], \tag{15}$$

where $ab=nk$ for the plus rate and $ab=lm$ for the minus rate and $\Lambda=\Lambda_{lmnk}=\hat{\sigma}^{(1)}_{s,lm}\hat{\sigma}^{(1)}_{s,nk}+\hat{\sigma}^{(1)}_{s,lm}\hat{\sigma}^{(2)}_{s,nk}+\hat{\sigma}^{(2)}_{s,lm}\hat{\sigma}^{(1)}_{s,nk}+\hat{\sigma}^{(2)}_{s,lm}\hat{\sigma}^{(2)}_{s,nk}$. For two distinct baths one finds analogously

$$\Gamma^{(\pm)}_{lmnk} = \frac{1}{8\hbar}[\Lambda^1 J_1(\omega_{ab})+\Lambda^2 J_2(\omega_{ab})][\coth(\beta\hbar\omega_{ab}/2)\mp 1] + \frac{i}{4\pi\hbar}[\Lambda^2 M_2^{\pm}(\omega_{ab})+\Lambda^1 M_1^{\pm}(\omega_{ab})], \tag{16}$$

with $\Lambda^1=\Lambda^1_{lmnk}=\hat{\sigma}^{(1)}_{s,lm}\hat{\sigma}^{(1)}_{s,nk}$, $\Lambda^2=\Lambda^2_{lmnk}=\hat{\sigma}^{(2)}_{s,lm}\hat{\sigma}^{(2)}_{s,nk}$ and

$$M_i^{\pm}(\Omega) = \mathcal{P}\int_0^\infty d\omega \frac{J_i(\omega)}{\omega^2-\Omega^2}[\coth(\beta\hbar\omega/2)\Omega\mp\omega], \tag{17}$$

where $\mathcal{P}$ denotes the principal value. The limit of ω_{ab} tending towards zero can be evaluated separately

$$\Gamma^{(+)}_{lmnk} = \Gamma^{(-)}_{lmnk} = \frac{\alpha}{4\beta\hbar}(\hat{\sigma}^{(1)}_{s,lm}\hat{\sigma}^{(1)}_{s,nk}+\hat{\sigma}^{(1)}_{s,lm}\hat{\sigma}^{(2)}_{s,nk}+\hat{\sigma}^{(2)}_{s,lm}\hat{\sigma}^{(1)}_{s,nk} + \hat{\sigma}^{(2)}_{s,lm}\hat{\sigma}^{(2)}_{s,nk}) \tag{18}$$

for one bath, and

$$\Gamma^{(+)}_{lmnk} = \Gamma^{(-)}_{lmnk} = \frac{1}{4\beta\hbar}(\alpha_1\hat{\sigma}^{(1)}_{s,lm}\hat{\sigma}^{(1)}_{s,nk}+\alpha_2\hat{\sigma}^{(2)}_{s,lm}\hat{\sigma}^{(2)}_{s,nk}) \tag{19}$$

for two baths. All calculations were performed in the same parameter regime as in Ref. [15], thus renormalization effects of the frequencies are weak and will be neglected. This structure of the rates nicely shows the relation to symmetry and DFS: The matrix elements of the $\hat{\sigma}_s$ in the eigenbasis determine the simultaneous symmetry properties of the qubit Hamiltonian and the system bath coupling. The energy splittings ω_{ab} determine the relevant segment of environmental phase space and depend on symmetry much more weakly.

IV. GATE QUALITY FACTORS

The ability of a realistic device, or in our case a more realistic model of a device, to operate a quantum gate is characterized by the four gate quality factors introduced in Ref. [30]. Those are the fidelity $\mathcal{F}$, purity $\mathcal{P}$, quantum degree $\mathcal{Q}$, and entanglement capability $\mathcal{C}$. The quantum degree and entanglement capability characterize entangling operations. They are unique to multiqubit gates. We will collectively refer to these as nonlocal gate quality factors (GQFs) as opposed to fidelity and purity, which are both well defined for an arbitrary number of qubits, in particular also for a single qubit, and will be referred to as the local gate quality factors.

The fidelity can be evaluated, following Ref. [24], as follows:

$$\mathcal{F} = \overline{\langle\Psi_{\text{in}}|U^\dagger\hat{\rho}_{\text{out}}U|\Psi_{\text{in}}\rangle}. \tag{20}$$

The overline indicates the average over a discrete set of unentangled input states $|\Psi_{\text{in}}\rangle$ that can serve as a basis for all possible input density matrices. The propagator U is the ideal unitary evolution of the desired gate, and $\hat{\rho}_{\text{out}}$ is the density matrix after applying the realistic gate to $|\Psi_{\text{in}}\rangle$. Thus a perfect gate reaches a fidelity of unity and the deviation from unity characterizes the deviation from the ideal process. The purity $\mathcal{P}$ is indicative of the decoherence effects

$$\mathcal{P} = \overline{\mathrm{tr}(\hat{\rho}_{\mathrm{out}}^2)}. \tag{21}$$

Again, the overbar indicates the input state average. A pure output state leads to $\mathcal{P}=1$, whereas as the state becomes increasingly mixed, the square of the weight of the contributions no longer sums up to unity and goes down to a minimum of one divided by the dimension of the Hilbert space of the system, 1/4 in our case.

Whereas the preceding two factors can be defined for any number of qubits, the following two are particular to the higher-dimensional case:

$$\mathcal{Q} = \max_{\rho_{\mathrm{out}},|\Psi_{\mathrm{me}}\rangle} \langle \Psi_{\mathrm{me}}|\rho_{\mathrm{out}}|\Psi_{\mathrm{me}}\rangle. \tag{22}$$

Here, the ρ_{out} are the density operators after the gate operation relating to unentangled input states, whereas the $|\Psi_{\mathrm{me}}\rangle$ are the maximally entangled states, also known as Bell states. Therefore, this measures the ability of the gate to create quantum entanglement.

Finally, the entanglement capability $\mathcal{C}$ is the smallest eigenvalue of the density matrix resulting from transposing the density matrix of one qubit. As shown in Ref. [31], the nonnegativity of this smallest eigenvalue is a necessary condition for the separability of the density matrix into two unentangled systems. After separation, the partially transposed density matrix is a valid density matrix as well, with nonnegative eigenvalues. The negativity of the smallest eigenvalue thus indicates that the states are not separable and therefore nonlocal. It approaches −0.5 for the ideal CNOT gate. The dynamics of entanglement in a two-qubit system has been studied in Ref. [32]. The entanglement capability is closely related to the *negativity* E_N of a state [33], which is a nonentropic entanglement monotone [34].

V. COMBINATION OF $\hat{\sigma}_x$ AND $\hat{\sigma}_z$ ERRORS

Now, the spin-boson model with a variable coupling operator to the harmonic oscillator baths, Eq. (10), is studied in more detail. We start with the CPHASE gate, which is entangling and forms the core part of the CNOT operation. The quantum degree for the CPHASE gate is always smaller than the ideal value because the CPHASE gate cannot create entangled Bell states in this particular basis. Thus, we did not consider the quantum degree for the CPHASE gate. The different error coupling configurations achieve the best gate quality factors for different coupling operators to the environmental baths. The scenarios are summarized in Table I.

TABLE I. Maxima of the gate quality factors for the CNOT and the CPHASE gate operation. Here T indicates the temperature and $T_S=E_S/k_B$ is the characteristic temperature scale, which corresponds to the qubit energy scale during the gate operation. Both the preferred bath configuration and qubit operator coupling to the bath are given.

CNOT	local GQFs	nonlocal GQFs	preferred case
$T \ll T_S$	close to $\hat{\sigma}_z$	close to $\hat{\sigma}_z$	1 bath
$T \gg T_S$	close to $\hat{\sigma}_z$	at $\hat{\sigma}_x$	1 bath
CPHASE	local GQFs	nonlocal GQFs	preferred case
$T \ll T_S$	at $\hat{\sigma}_z$	at $\hat{\sigma}_z$	—[a]
$T \gg T_S$	at $\hat{\sigma}_z$	at $\hat{\sigma}_x$	2 baths

[a]There is no clear tendency observed in this case, see Fig. 1. Close to pure $\hat{\sigma}_z$ coupling two baths are preferred, and close to $\hat{\sigma}_x$ one bath.

Two qualitatively different temperature regimes are found, separated by a smooth crossover. Temperatures are measured in units of T_s, where $E_S/h=(k_B/h)T_S$ is the characteristic energy scale, which corresponds to the typical qubit energy scale during the quantum gate operation and is typically of the order of a few GHz. For low temperatures $T \ll T_S$, spontaneous emission processes dominate. When T_S is approached, thermal effects become important and for $T \approx T_S$ temperature is the dominating energy scale as will be discussed in more detail below.

The CPHASE gate, for pure $\hat{\sigma}_z$ coupling, is protected by symmetry because the gate operation and the coupling to the bath commute. As was shown previously, all disturbances vanish here in the limit of low temperatures. In this case,

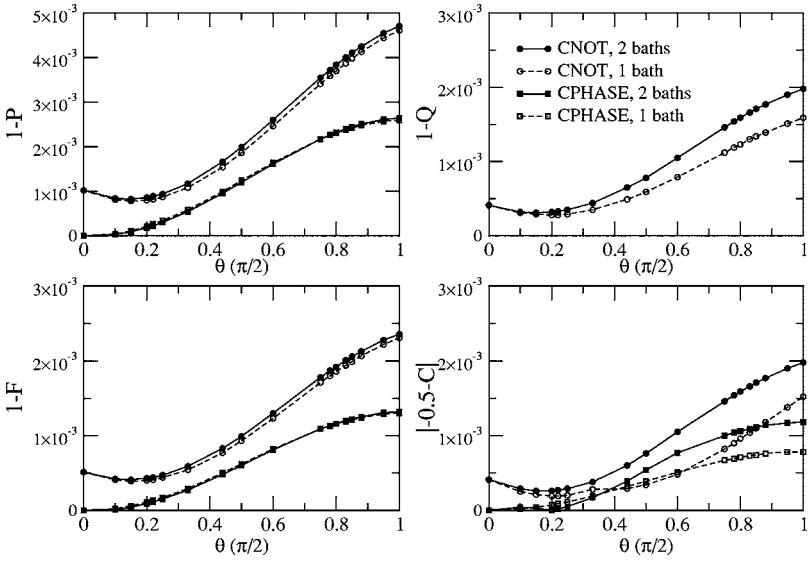

FIG. 1. Dependence of the gate quality factors on the bath coupling angle θ defined in Eq. (10) for the CNOT and CPHASE operation at $T \approx 0 \ll T_S$. Here, the behavior of the gate quality factors for both the single bath and two bath case is shown. The characteristic energy scale for the gate operation is $E_S/h=1$ GHz [15]. The lines are provided as guides to the eye.

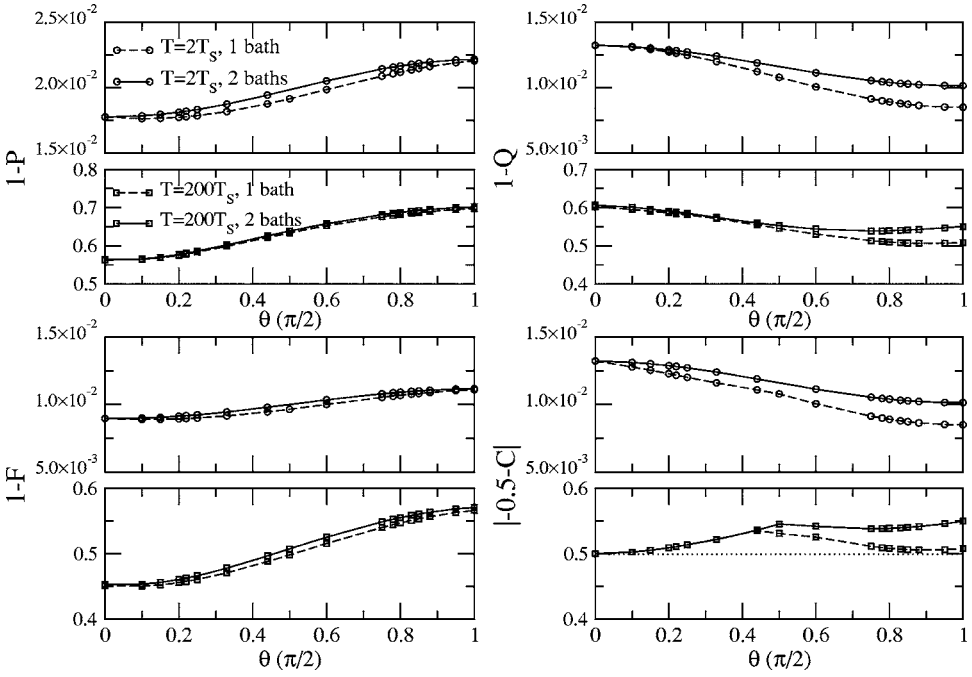

FIG. 2. Dependence of the gate quality factors on the bath coupling angle θ defined in Eq. (10) for the CNOT operation at large temperatures $T=2T_S$ and $T=200T_S$. The characteristic energy scale for the gate operation is $E_S/h=1$ GHz [15]. The lines are provided as guides to the eye.

spontaneous emission processes are the dominating decoherence mechanism because absorption and excitation processes are effectively suppressed due to the bath coupling (i.e., matrix elements for theses processes are restricted due to symmetries of the bath coupling operators) and the temperature. In this case, the low-temperature regime can be referred to as the emission limited regime.

The additional $\hat{\sigma}_x$ operation in the CNOT gate Eq. (4) during the single qubit Hadamard operations leads to nonvanishing decoherence rates even in the low-temperature limit. The reason is again the competition of pure dephasing with emission and absorption processes which show a different dependence on the coupling angle θ.

However, the Hadamard part of the CNOT operation is short compared to the overall length of the gate operation (4). Thus, it is found that for low temperatures the best values for the GQFs are obtained very close to pure $\hat{\sigma}_z$ coupling as depicted in Fig. 1. This implies that the overall decoherence effects are smallest if the bath coupling angle θ throughout the gate is adjusted to the distribution of gate operations, which are characterized by different directions on the Bloch sphere.

For the CNOT gate better results are observed for the single bath case throughout the low-temperature regime, see Fig. 1. For the single bath configuration, close to pure $\hat{\sigma}_x$ coupling to the bath, the difference becomes quite significant and for the nonlocal GQFs actually approaches a factor of 2, but reduces again as pure $\hat{\sigma}_x$ coupling is reached. The CPHASE gate (see Fig. 1) prefers a two bath configuration unless the coupling is $\hat{\sigma}_x$ dominated. Again, the nonlocal GQFs are affected most.

For the pure $\hat{\sigma}_z$ case ($\theta=0$ or correspondingly $c_x=c_y=0$ and $c_z=1$) little difference between the two bath and the single bath behavior is found in the CNOT case and none at all for the CPHASE. It is observed that the single bath configuration is certainly preferred as soon as there is a significant $\hat{\sigma}_x$ contribution in the gate operation. This means that the additional protection from the one-dimensional decoherence free subspace [15,16] involved is mainly beneficial if the commutator of the qubit operator, which couples to the bath and the qubit Hamiltonian (the Hamiltonian that is needed to perform the individual parts of the gate operation) has appropriate matrix elements, i.e., if there is a significant noncommuting part in the bath coupling and the gate operations. However, in a $\hat{\sigma}_z$ dominated case the individual coupling is preferred as it does not induce any additional indirect couplings between the qubits. It is natural that the two qubit GQFs should notice this more strongly than the single qubit GQFs for which the differences never become more than about one fifth of the individual deviations.

For the high-temperature regime, drastically different behavior in the nonlocal GQFs is found, see Fig. 2. Both Q and C now achieve their best values at a pure $\hat{\sigma}_x$ coupling for both gates, the local GQFs achieve their maximum at a pure $\hat{\sigma}_z$ value. The protection that the CPHASE gate enjoyed in the low temperature regime breaks down here. The high-temperature case is essentially scale free, i.e., high temperatures symmetrize the system. In this case the system eigenbasis is given by the qubit operator which couples to the bath. This can be nicely shown when considering the single qubit dephasing rates within the spin-boson model [21]

$$\Gamma_\varphi = \frac{1}{T_2} = \frac{\epsilon^2}{2E^2}S(0) + \frac{\Delta^2}{2E^2}S(E), \tag{23}$$

where E is the single qubit energy splitting and $S(E)$ denotes the power spectrum of the noise. The expression Eq. (23) becomes $\Gamma_\varphi \approx 2\pi\alpha k_B T/\hbar$ for $T \gg E$ and does not depend on the ratio Δ/ϵ.

Thermalization is determined by the off-diagonal bath couplings in the basis of the corresponding system Hamiltonian which is required for a certain gate operation. It will

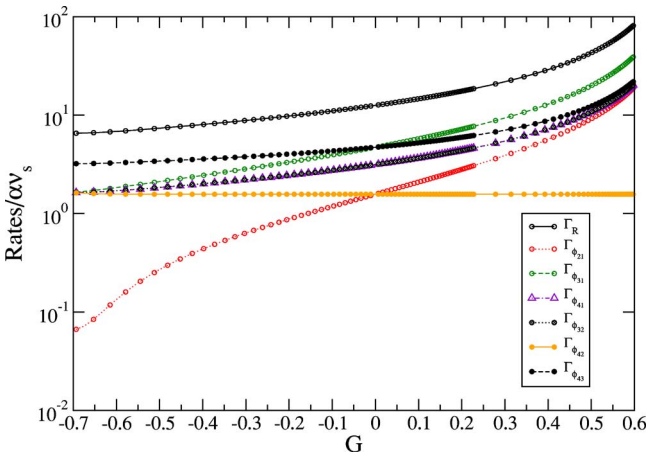

FIG. 3. (Color online) Dependence of the decoherence rates on the qubit asymmetry. Here, we set $K=0$, $\epsilon_i=0$, $\Delta_2=E_S$, and vary Δ_1. The single and two bath cases behave identically, thus only the single bath case is shown. The strength of the decoherence effects is set to $\alpha=10^{-3}$ and $T\approx 0.5T_S$. We set the bath coupling angles (24) to $\theta_1=0$ and $\theta_2=0$, i.e., the bath coupling operator and the Hamiltonian are perpendicular. The decoherence rates are scaled by $\alpha\nu_S$, with $\nu_S=E_S/h$. The lines are provided as guides to the eye.

be strongly dominated by the noncommuting contributions, i.e, the $\hat{\sigma}_x$ bath coupling for the CPHASE part of the CNOT gate. The single qubit Hadamard part of the CNOT gate will be additionally also affected by the $\hat{\sigma}_z$ bath coupling. The two-qubit operation (CPHASE), or in other words the nonlocal part, of the CNOT gate is of the $\hat{\sigma}_z^{(1)}\hat{\sigma}_z^{(2)}$ type and the single qubit Hadamard gates contain both $\hat{\sigma}_x$ and $\hat{\sigma}_z$ contributions. Thus, during the gate operation the thermalization is dominated strongly by the $\hat{\sigma}_x$ part of the bath coupling for the nonlocal and by the $\hat{\sigma}_z$ part for the local GQFs, implying that for thermal fluctuations the $\hat{\sigma}_x$-type couplings are more important in inducing interqubit transitions, while $\hat{\sigma}_z$ primarily affects the single qubit gate quantifiers. What implementation to choose for a gate here, becomes a question of what gate quantifiers are desired to be optimized. The differences between the one bath and two bath scenario are now small.

For pure $\hat{\sigma}_z$ coupling of the qubit to the bath, a peculiar effect is observed. In this case, the minimal eigenvalue of the partially transposed density matrix that is the entanglement capability remains negative even for $T \gg T_s$ (Fig. 2). The negativity of the eigenvalue of the partially transposed density matrix is not just a necessary but also a sufficient criterion for the nonseparability of the system in our case [31]. Thus, no matter what the temperature or strength of the dissipative effects in our system during the CNOT gate operation, entanglement will never be eliminated completely. This can be explained by rapid thermalization into a protected entangled state. Furthermore, this effect carries over well into the regime where both $\hat{\sigma}_x$ and $\hat{\sigma}_z$ noise are present.

Overall, the temperature (and the coupling strength) has the largest influence on the GQFs. At $T \ll T_s (T \approx 10^{-3}$ K), we observe deviations of the GQFs from the ideal value which are less than 10^{-3}. At $T \gg T_s (T \approx 1$ K) the deviations are 10^{-1} and quickly increasing further at larger temperatures. The different coupling operators to the bath are the next strongest effect. Rotating the coupling operator from $\hat{\sigma}_z$ to $\hat{\sigma}_x$ causes, in the worst cases, three to four times stronger deviations from the ideal value than the $\hat{\sigma}_z$ noise. Finally, the change due to different types of bath couplings is generally small compared to the differences between $\hat{\sigma}_x$ and $\hat{\sigma}_z$ type coupling. This also suggests that we do not need to worry about noise sources with at least one order of magnitude weaker coupling strength, even if they couple through a less favorable coupling operator.

As an intermediate conclusion, it is found that for the decoherence dominated regime the CPHASE operation reached the optimum value of the GQFs for a pure $\hat{\sigma}_z$ coupling to the bath. In the case of the CNOT operation, the minimum is located slightly shifted to the $\hat{\sigma}_x$ component because of the mixture of $\hat{\sigma}_x$ parts during the Hadamard operations, compare with Fig. 1. For the CNOT operation, the optimum values of the four gate quantifiers are encountered at different bath couplings, which are characterized by the mixing angle Eq. (10), especially for large temperatures.

Thus, the differences between the case of one common bath and two baths are much less important than the symmetries between the gate operation and the bath operators. In particular, the difference between the case of one or two baths disappears for pure $\hat{\sigma}_z$ coupling to the bath. Here, decoherence due to flux noise or charge noise in coupled superconducting flux or charge qubits was explored. Decoherence due to $1/f$ noise, caused by background charges or bistable fluctuators, was not treated. If still in the motional narrowing limit, it can be included in the Redfield equations by introducing a peak at zero frequency in the spectral function with a magnitude given by experiment [35]. More generally, microscopic calculations are needed [36].

VI. NONIDENTICAL QUBITS

Now, we do not restrict the analysis to the case of a uniform error coupling Eq. (10) anymore. In general, both qubits can couple to the baths differently

$$\hat{\sigma}_s^{(i)} = \hat{\sigma}_x^{(i)} \sin\theta_i + \hat{\sigma}_z^{(i)} \cos\theta_i, \tag{24}$$

where $i=1,2$ denotes one of the qubits. For the numerical calculations, the qubits are set to the degeneracy point $K=\epsilon_i=0$ and Δ_2 is set to E_S, i.e., effectively this model describes a system of two uncoupled qubits. Here, Δ_1 and thus also the asymmetry $G=(\Delta_1-\Delta_2)/(\Delta_1+\Delta_2)$ is varied.

Experimentally the spread of the qubit parameters due to fabricational imprecision is very important both because quantum algorithms (without further modification) require a certain level of precision and the decoherence effects in the system of qubits have to be sufficiently small [37].

Therefore, it is of central importance to investigate also the effects of the parameter spread in nonidentical qubits on the behavior of the decoherence rates. Superconducting qubits are preferably operated at the degeneracy point where decoherence effects are suppressed for superconducting charge and flux qubits. However, the tunnel matrix elements for superconducting qubits can differ significantly, on the order of several percent [12,14]. Thus, the dependence of the decoherence rates, i.e., dephasing rates and the relaxation

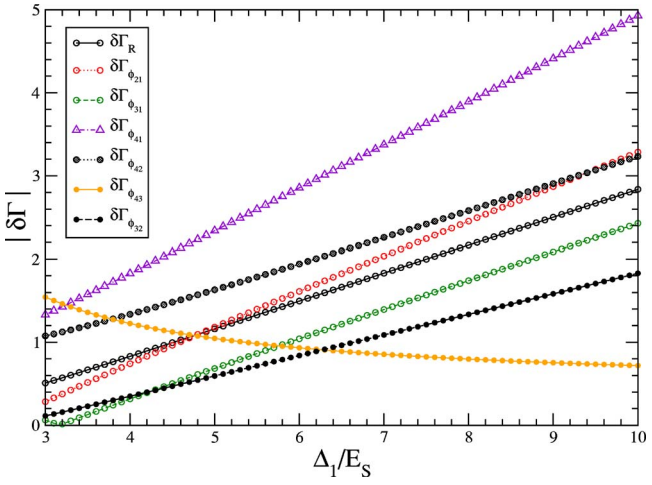

FIG. 4. (Color online) Dependence of the decoherence rates on the qubit asymmetry at $T \approx 0.5T_S$. Here, the case of one common bath is investigated. The tunnel matrix element of the second qubit and the interqubit coupling are set to $\Delta_2 = K = E_S$ and Δ_1 is varied. For comparison with experiments, large asymmetry in the tunnel matrix elements of the individual qubits is investigated. The bath coupling angles are set to $\theta_1 = 0$ and $\theta_2 = 0$. The strength of the dissipative effects is $\alpha = 10^{-3}$. The lines are provided as guides to the eye.

rate, close to the degeneracy point on the qubit asymmetry is an important property. The decoherence rates are defined according to Refs. [26,15]. Namely, the relaxation rate is $\Gamma_R = -\Sigma_n \Lambda_n$, where Λ_n are the eigenvalues of the matrix $R_{n,n,m,m}$, $n,m = 1,\ldots,4$, and the dephasing rates are $\Gamma_{\varphi_{nm}} = -\mathrm{Re} R_{n,m,n,m}$.

Figure 3 depicts the dependence of the decoherence rates on the qubit asymmetry G when the individual qubits are operated close to the degeneracy point. A Temperature $T \approx 0.5T_S$, which is typical for experimental situations, is chosen for this analysis.

We observe that for pure $\hat{\sigma}_x$ coupling to the bath ($\theta_1 = \pi/2$ and $\theta_2 = \pi/2$), the asymmetry of the qubits is irrelevant because the coupling to the bath and the system Hamiltonian commute (the indices of qubit one and qubit two could be exchanged without changing the system). For mixed bath coupling of the $\hat{\sigma}_x$ type for one qubit ($\theta_1 = \pi/2$) and the $\hat{\sigma}_z (\theta_2 = 0)$ type for the other qubit, still the decoherence rates do not vary for different asymmetry. The reason for this behavior is that the $\hat{\sigma}_x$ bath coupling of the first qubit *always* commutes with the qubit Hamiltonian, i.e., only flipless dephasing processes contribute to the decoherence rates of the first qubit. When we vary the asymmetry, essentially Δ_1 is varied ($\Delta_2 = E_S$ is kept constant), which leads to a different contribution of the first qubit to the overall decoherence. However, these corrections are small compared to the full decoherence rates (i.e., not only flipless dephasing processes) that contribute in the case of qubit two where $[H_{\mathrm{SB}}, H_{\mathrm{sys}}] \neq 0$ and Δ_2 stays constant.

Finally, Fig. 3 shows the case of exactly perpendicular system Hamiltonian and bath coupling. Here, the decoherence rates increase steeply for increasing asymmetry. Note here that due to the definition of G and Δ_2, the two cases $G = -0.6 \rightarrow \Delta_1 = (1/4)E_S$ and $G = 0.6 \rightarrow \Delta_1 = 4E_S$ are vastly different.

From the dependence of the decoherence rates on the asymmetry G of the two qubits at the degeneracy point, it is possible to estimate the maximum tolerable asymmetry for a given constraint on the deviation of the decoherence rates from their value for perfectly symmetric qubits. It is found that in order for the deviation of the relaxation rate from its value for perfectly symmetric qubits to stay below 1%, it is required that $0.5\Delta_2 < \Delta_1 < 1.5\Delta_2$; i.e., the parameter spread of the two qubits could be remarkably large ($\approx 50\%$) without considerably affecting the relaxation rates. However, detailed analysis shows that for the deviations of the dephasing rates, the increase happens much earlier. Moreover, there is a large spread among the dephasing rates, which are sensitive to the qubit asymmetries. Note that both the single bath and the two bath case behave identically for the relaxation rate. Differences between the two cases only occur for the dephasing rates. The angles of the bath coupling where the minimum dephasing rates are encountered are different for the different dephasing rates.

Typical experimental values for charge [12] and flux qubit [14] designs indicate that the parameter spread in the tunnel matrix amplitudes can be quite large, in the case of the charge qubit it is a factor of $\Delta_2/\Delta_1 \approx 0.91$ and for the flux qubit $\Delta_2/\Delta_1 \approx 4.22$, which corresponds to deviations of approximately ten and up to several hundred percent, respectively. This difference of asymmetries is due to the fact, that fabrication parameters such as E_c and E_J enter the *exponent* of the tunnel splitting in the flux qubit case [6]. Thus, the parameter spread of the tunneling amplitudes for the flux qubit is larger and the decoherence rates will be considerably affected. These experimental values emphasize that it is important to study the evolution of the decoherence effects for nonidentical qubit parameters. Moreover, important information about the noise sources coupling to the qubit can be identified. From comparison of the decoherence rates for different qubit samples, which possess different asymmetries between the tunnel amplitudes, it is thus possible to identify the predominant bath coupling angle. In most qubit designs the bath coupling angle is then uniquely related to a certain noise source, e.g., flux noise in the case of flux qubits [38].

Figure 4 depicts the experimentally important [14] behavior of the decoherence rates when Δ_2 and K are fixed to E_S and $\Delta_1 > \Delta_2$ is changed. We define the deviation of the decoherence, i.e., the relaxation or dephasing rates from their values at the degeneracy point as

$$\delta\Gamma_{R,\varphi_{ij}} = 1 - \frac{\Gamma_{R,\varphi_{ij}}(\Delta_1 \neq \Delta_2, K = E_S, \epsilon_i = 0)}{\Gamma_{R,\varphi_{ij}}(\Delta_1 = \Delta_2 = K = E_S, \epsilon_i = 0)}. \quad (25)$$

In this case the two qubits are permanently coupled, and embedded into one common environmental bath. The decoherence rates begin to increase linearly when Δ_1 is larger than Δ_2.

Figure 5 illustrates the temperature dependence of the decoherence rates for the case of one common bath. The values of the decoherence rates for the two bath case differ insignificantly from the single bath case. We observe that the

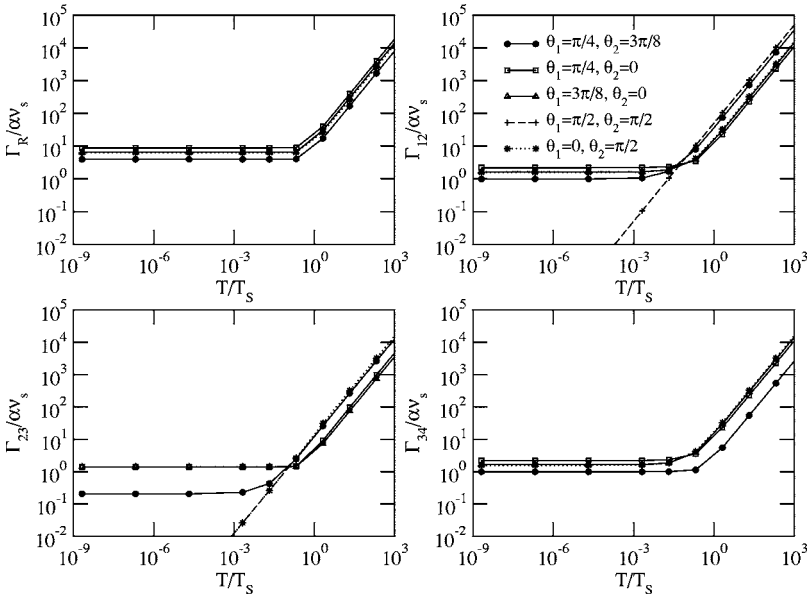

FIG. 5. Temperature dependence of selected decoherence rates for $K=0$, $\epsilon_i=0$, $\Delta_1=E_S$, $\Delta_2=0.9\Delta_1$, for the single bath case. Here, temperature and the bath coupling angles are varied. The strength of the dissipative effects is set to $\alpha=10^{-3}$. The decoherence rates are scaled by $\alpha\nu_S$, where $\nu_S=E_S/h$. The lines are provided as guides to the eye.

spread of the magnitude of the different decoherence rates increases at intermediate mixing angles. As expected, the magnitude of the decoherence rates is maximum in the case where the system Hamiltonian and the coupling to the bath are perpendicular to each other. For the opposite case, where the system Hamiltonian and the coupling to the bath commute, the decoherence rates vanish for decreasing temperature, i.e., only flipless dephasing processes contribute to the overall decoherence. Note that in the case where the system Hamiltonian and the coupling to the bath commute ($\theta_1=\pi/2$ and $\theta_2=\pi/2$) the relaxation rate vanishes.

It is found that the dephasing rates depend strongly on the qubit asymmetry. Nevertheless the parameter spread of the qubit energies can be quite large (around 10%) without affecting the decoherence properties considerably for the case of a favorable bath coupling. However, for very large asymmetries and a bath coupling, which is perpendicular to the system Hamiltonian, the decoherence rates increase exponentially with asymmetry.

VII. CONCLUSION

A system of two pseudospins coupled by an Ising-type $\hat{\sigma}_z^{(1)}\hat{\sigma}_z^{(2)}$ interaction, which models e.g., superconducting charge or flux qubits, was investigated. It was shown that for the system of two pseudospins the optimum gate performance of different gate operations is closely related to their composition of elementary gates and the coupling to the bath. In more detail, the gate fidelity is enhanced when the coupling angle to the bath imitates the composition of the gate operation in terms of Hamiltonian parts pointing in different directions on the Bloch sphere. When considering the gate quality factors, the temperature and aforementioned special symmetries of the system-bath coupling have a large influence on the decoherence properties, whereas the differences for the single or two bath scenarios are minor. For the CPHASE operation at low temperatures, the optimum gate quality factors are at pure $\hat{\sigma}_z$ system-bath coupling due to the fact that only in this case all individual Hamiltonians necessary for performing the gate operations and the system bath coupling commute. Similarily, the CNOT gate operation approaches the best gate quality factors close to $\hat{\sigma}_z$ system-bath coupling with a slight $\hat{\sigma}_x$ admixture due to the Hadamard operations. These findings can be directly applied in systems where it is possible to engineer the decohering environment to a certain degree [39]. Moreover, special symmetries that are identified in experiments can also be used for the encoding of several physical qubits into logical qubits [16,17] to reduce the effects of the environmental bath.

For very large temperatures, the temperature effectively symmetrizes the system and thus entanglement is always preserved during a CNOT gate operation independently of the system-bath coupling. It is found that the parameter spread of the tunnel matrix elements of the qubits, when operated close to the degeneracy point can be quite large (approximately 10%) for a bath coupling which *commutes* with the system Hamiltonian without affecting the decoherence properties considerably; which again emphasizes the importance of using the symmetry properties of the system and bath to improve the decoherence of the qubit system. In the special case where the system Hamiltonian commutes with the system-bath coupling Hamiltonian, the differences in the decoherence rates stay below 1% for the aforementioned spread of the tunnel matrix elements. This special case can model the situation in superconducting flux qubits [13,14], where the dominating noise source is flux noise, quite well if the tunnel matrix elements of the individual qubits are small compared to the energy bias of the qubits and the interqubit coupling strength. However, in a more general setup with nonidentical qubits, the aformentioned symmetry properties are almost certainly not fulfilled and the performance of the qubits will be degraded quite significantly.

VIII. OUTLOOK

Our results indicate, that in case of tunable bath coupling operators, decoherence may be further engineered. Moreover, they indicate that symmetry-induced coherence protec-

tion is remarkably stable under realistic parameter spread. These results are expected to have significant impact on the analysis of the recent experiments [9,14,19]. Next to its practical importance, this emphasizes the role of the spatial correlations of the environmental noise that has been assumed here, but which needs to become an integral part of the experimental characterization of the environment.

ACKNOWLEDGMENTS

This work was supported in part by DFG through SFB 631 and by NSA and ARDA under ARO Contract No. P-43385-PH-QC. We thank A.B. Zorin, W.D. Oliver, A. Marx, L.C.L. Hollenberg, S. Kohler, U. Hartmann, M. Mariantoni, and S. Ashhab for useful discussions.

[1] P. Shor, in *Proceedings of the 35th Annual Symposium on the Foundations of Computer Science*, edited by S. Goldwasser (IEEE Computer Society Press, Los Alamitos, California, 1994), pp. 124–134.
[2] L. K. Grover, Phys. Rev. Lett. **79**, 325 (1997).
[3] D. Deutsch, Proc. R. Soc. London, Ser. A **400**, 97 (1985).
[4] D. P. DiVincenzo, Science **269**, 225 (1995).
[5] M. A. Nielsen and I. L. Chuang, *Quantum Computation and Quantum Information* (Cambridge University Press, Cambridge, 2000).
[6] T. P. Orlando *et al.*, Phys. Rev. B **60**, 15398 (1999); J. E. Mooij *et al.*, Science **285**, 1036 (1999).
[7] C. H. van der Wal, Ph.D. thesis, TU Delft, Delft, 2001.
[8] Yu. A. Pashkin, T. Yamamoto, O. Astafiev, Y. Nakamura, D. V. Averin, and J. S. Tsai, Nature (London) **421**, 823 (2003).
[9] Y. Nakamura, Yu. A. Pashkin, and J. S. Tsai, Nature (London) **398**, 786 (2002).
[10] D. Vion, A. Aassime, A. Cottet, P. Joyez, H. Pothier, C. Urbina, D. Esteve, and M. H. Devoret, Science **296**, 886 (2002).
[11] I. Chiorescu, Y. Nakamura, C. J. P. M. Harmans, and J. E. Mooij, Science **299**, 1869 (2003).
[12] T. Yamamoto, Y. A. Pashkin, O. Astaviev, Y. Nakamura, and J. S. Tsai, Nature (London) **425**, 941 (2003).
[13] A. C. J. ter Haar, Ph.D. thesis, TU Delft, Delft, 2005.
[14] J. B. Majer, F. G. Paauw, A. C. J. ter Haar, C. J. P. M. Harmans, and J. E. Mooij, Phys. Rev. Lett. **94**, 090501 (2005).
[15] M. J. Storcz and F. K. Wilhelm, Phys. Rev. A **67**, 042319 (2003).
[16] J. Kempe, D. Bacon, D. A. Lidar, and K. B. Whaley, Phys. Rev. A **63**, 042307 (2001).
[17] M. J. Storcz, J. Vala, K. R. Brown, J. Kempe, F. K. Wilhelm, and K. B. Whaley, Phys. Rev. B **72**, 064511 (2005).
[18] D. Bacon, D. A. Lidar, and K. B. Whaley, Phys. Rev. A **60**, 1944 (1999).
[19] A. B. Zorin, JETP **98**, 1250 (2004).
[20] J. R. Friedman, V. Patel, W. Chen, S. K. Tolpygo, and J. E. Lukens, Nature (London) **406**, 43 (2000).
[21] Y. Makhlin, G. Schön, and A. Shnirman, Rev. Mod. Phys. **73**, 357 (2001).
[22] J. Q. You, Y. Nakamura, and F. Nori, Phys. Rev. B **71**, 024532 (2005).
[23] Yu. A. Pashkin, T. Yamamoto, O. Astafiev, Y. Nakamura, D. V. Averin, and J. S. Tsai, Nature (London) **421**, 823 (2003).
[24] M. Thorwart and P. Hänggi, Phys. Rev. A **65**, 012309 (2002).
[25] I. A. Grigorenko and D. V. Khveshchenko, Phys. Rev. Lett. **94**, 040506 (2005).
[26] M. Governale, M. Grifoni, and G. Schön, Chem. Phys. **268**, 273 (2001).
[27] K. Rabenstein and D. V. Averin, Turk. J. Phys. **27**, 1 (2003).
[28] U. Weiss, *Quantum Dissipative Systems*, 2nd ed. (World Scientific, Singapore, 1999).
[29] K. Blum, *Density Matrix Theory and Applications*, 1st ed. (Plenum, New York, 1981).
[30] J. F. Poyatos, J. I. Cirac, and P. Zoller, Phys. Rev. Lett. **78**, 390 (1997).
[31] A. Peres, Phys. Rev. Lett. **77**, 1413 (1996).
[32] V. M. Aji and J. E. Moore, cond-mat/0312145.
[33] K. Zyczkowski, P. Horodecki, A. Sanpera, and M. Lewenstein, Phys. Rev. A **58**, 883 (1998).
[34] J. Eisert, Ph.D. thesis, University of Potsdam, Potsdam, 2001.
[35] O. Astafiev, Yu A. Pashkin, Y. Nakamura, T. Yamamoto, and J. S. Tsai, Phys. Rev. Lett. **93**, 267007 (2004).
[36] G. Falci, A. D'Arrigo, A. Mastellone, and E. Paladino, Phys. Rev. Lett. **94**, 167002 (2005).
[37] D. Aharonov and M. Ben-Or, quant-ph/9906129.
[38] C. H. van der Wal, F. K. Wilhelm, C. J. P. M. Harmans, and J. E. Mooij, Eur. Phys. J. B **31**, 111 (2003).
[39] F. K. Wilhelm, M. J. Storcz, C. H. van der Wal, C. J. P. M. Harmans, and J. E. Mooij, Adv. Solid State Phys. **43**, 763 (2003).